

What drives the seasonal onset and decay of the Western Hemisphere Warm Pool?

S.-K. Lee¹, D. B. Enfield² and C. Wang²

¹ Cooperative Institute for Marine and Atmospheric Studies, University of Miami, Miami FL

² Atlantic Oceanographic and Meteorological Laboratory, NOAA, Miami FL

Submitted to Journal of Climate

March 2004

Version 1.6

ABSTRACT

The annual heat budget of the Western Hemisphere Warm Pool (WHWP) is explored using the output of an Ocean General Circulation Model (OGCM) simulation. According to our analysis, the WHWP cannot be considered as a monolithic whole with a single set of dominating processes that explain its behavior. The four regions considered, namely the eastern north Pacific (ENP), the Gulf of Mexico (GoM), the Caribbean Sea (CBN) and the equatorial Atlantic (EQA), are each unique in terms of the atmospheric and/or oceanic processes that dominate the corresponding heat budgets. In the ENP region increased cloud cover in boreal summer and associated reduction in solar radiation plays a crucial role for the warm pool's demise, while ocean upwelling in the Costa Rica Dome connected to surrounding areas by horizontal advection offers a persistent yearlong cooling mechanism. A process of winter convection that warms the upper layer marks the Gulf of Mexico. The Caribbean is affected by vertical and horizontal advective cooling within and away from the coastal upwelling zone off northern South America during the onset and peak phases, slowing down the warming considerably. Advective processes associated with the equatorial cold tongue dominate the EQA region. Turbulent mixing is an important cooling mechanism in the annual cycle of the WHWP, and we find some evidence that the mixing is sustained by the mean shear at the warm pool base. Common to all four WHWP regions is the reduction of wind speed in the peak phase, suggestive of a convection-evaporation feedback known to be important in the Indo-Pacific warm pool dynamics. High-resolution model simulations along with available observational data are needed to validate the findings in this study.

1. Introduction

The Western Hemisphere Warm Pool (WHWP) is a warm body of surface water that appears between March and October in the western hemisphere over the eastern north Pacific (ENP), the equatorial Atlantic (EQA), the Gulf of Mexico (GoM) and the Caribbean Sea (CBN) (Wang and Enfield, 2001). During its warming (onset) phase, the WHWP receives heat from the atmosphere expanding its boundary to its surrounding ocean. Once it is fully charged, the WHWP releases a massive amount of moisture into the overlying atmosphere, thus affecting the deep tropical convection in the western hemisphere (Wang and Enfield, 2003), and the rainfall over the continental United States and Central America (Bosilovich, 2002).

In previous work, Enfield and Lee (2005, EL05 hereafter) showed that the seasonal warming of the WHWP is largely forced by the shortwave radiation cycle (with modification by cloud cover in the ENP), while the latent heat flux plays a secondary but important role particularly during the cooling (decay) phase. EL05 also showed that the diffusive heat exchange with the cooler surroundings is the major damping mechanism of the warm pool, with its rate in the range between -4.3 and -23.6W/m^2 , and that the advective heat flux divergence plays a relatively minor role in the ENP and GoM subregions, with its rate between -5.5 and -2.0W/m^2 . These findings are consistent with Niiler and Stevenson (1982) who suggested that, because the water that enters a warm pool has the same temperature as the water that leaves it, turbulent mixing is the only mechanism that damps out the large net heat gain at the sea surface. However, two shortcomings in EL05 must be noted: (1) the rate of oceanic advective heat flux divergence obtained in EL05 was subject to large errors due to the sparseness of the surface drifter data, and (2) the diffusive heat flux was estimated indirectly through heat equation residuals. Unlike the Indo-Pacific warm pool, which is large year-round, the WHWP is highly time-dependent as it appears only for four

months in the ENP and EQA and shifts to the GoM then to the CBN and lasts there for another four months. Since the warm pool thermodynamics envisioned by Niller and Stevenson (1982) are valid strictly for the steady-state condition, the heat budget of the WHWP is less likely to be dictated by the isothermal condition along the warm pool boundary. This leads us to suspect that the advective heat flux divergence is important in the WHWP cycle, at least in certain subregions.

In order to surmount the shortcomings of EL05 and to assess the dominant forcing and damping mechanisms that operate in the WHWP, we explore the annual heat budget cycle of the WHWP using the output from the Hybrid Coordinate Ocean Model (HYCOM) simulation (Lee et al., 2005, henceforth LEW05), with particular emphasis on the impact of oceanic advective heat flux divergence. To properly assess the impact of the ocean dynamics, we use the 27.5°C isotherm to locate the approximate positions and boundaries of the warm pool slabs, then the heat conservation equation is volume-integrated to derive the so-called slab heat budget equation, which is in turn applied to the twelve monthly outputs from HYCOM simulation. In the following sections, after briefly describing the HYCOM simulation (section 2), the slab heat budget equation is derived (section 3) and the dominant air-sea processes responsible for the forcing and damping of the four WHWP regions are discussed based on the slab heat budget analysis (section 4). In section 5, the model-generated values of diffusive and advective heat flux are compared with those of EL05, and a summary and discussion is provided in section 6.

2. HYCOM simulation

The details on HYCOM configuration are documented in LEW05, and thus are summarized only briefly here. The model domain contains both the Pacific and Atlantic Oceans between

100°E and 20°E, bounded north and south by 65°N and 35°S, respectively. The grid resolution is uniform 1° zonally and variable in the meridional direction; 0.5° at the equator increasing linearly to 1° at 40° latitude and remaining 1° poleward of 40°. In the vertical, 22 non-uniform hybrid layers are used. The grid structure in the eastern tropical Pacific and the tropical Atlantic, and the locations of the four subregions of the WHWP, are indicated in Figure 1. The constrained Southampton surface flux climatology (SHC, Grist and Josey, 2003), which is least-biased over the WHWP regions (EL05; LEW05), is used to force HYCOM. The K-Profile Parameterization (KPP) scheme of Large et al. (1994) is used to parameterize the vertical turbulent mixing. The time- and space-dependent light attenuation depth is derived from space-based ocean color measurements. The WHWP SST bias in the fine-tuned case ranges between -0.41 and 0.18°C. See LEW05 and Halliwell (2004) for more discussion about HYCOM's sensitivities to surface flux data and other model parameterizations.

HYCOM mainly uses the potential density as the vertical coordinate, but it allows the vertical coordinate to become pressure-like near the ocean surface, and uses the sigma coordinate in shallow water regions. The major advantage of using such a complex vertical coordinate system is to provide appropriate vertical resolution in the surface mixed layer and shallow water area. However, one trade-off is that HYCOM uses the so-called hybrid grid generator, which is a numerical scheme that reconstructs the layer structure during the model integration to match the predefined target density of each layer (Bleck, 2002). The hybrid grid generator acts like an "upstream" vertical advection operator, which is known to be diffusive (Bleck, 2002). Numerical diffusion of such nature can have serious consequences in the heat tendency of the non-isopycnal layers. Therefore, an anti-diffusion scheme is introduced in the latest HYCOM release (version 2.1) to minimize the numerical diffusion. In this study, however, instead of applying the anti-

diffusion scheme, we simply finesse the problem by forcing the non-isopycnal layers to have prefixed depths throughout the model integration. In this way, the hybrid grid generator causes no numerical diffusion in our simulation. For more detailed description and recent development of HYCOM on this and other issues, see Bleck (2002) and Halliwell (2004).

3. Slab heat budget equation

Integration of the heat conservation equation over a regional warm pool slab bounded by the sea surface and the fixed side and bottom boundaries (Figure 1) yields

$$\underbrace{\frac{d}{dt} \iiint \rho c_p T dV}_{Q_{STR}} = \underbrace{\iint R|_{z=0} dA + Q_{LAT} + Q_{SEN}}_{Q_{NET}} - \underbrace{\iint R|_{z=-d} dA}_{Q_{SWP}} + \underbrace{\iint \rho c_p T \mathbf{v} \cdot \mathbf{n} dA}_{Q_{ADV}} + \underbrace{\iint \frac{\partial \overline{w' T'}}{\partial z} \Big|_{z=-d} dA}_{Q_{DIF}}, \quad (1)$$

where ρ is the water density, c_p is the specific heat of sea water, $\mathbf{v} \cdot \mathbf{n}$ is the velocity component normal to the warm pool's side and bottom boundaries, R is the radiative heat flux at a given depth and d is the slab depth. The LHS is the heat storage rate (Q_{STR}), the RHS includes the surface net heat flux (Q_{NET}), the shortwave penetration at the slab base (Q_{SWP}), the advective heat flux divergence (Q_{ADV}) and the diffusive heat flux across the slab base (Q_{DIF}), respectively. Note that the horizontal sub-grid diffusion term, although it is a part of the model heat equation, is not included in (1) because it is usually very small.

The surface net heat flux can be written as

$$Q_{NET} = Q_{SWR} + Q_{LWR} + Q_{LAT} + Q_{SEN}, \quad (2)$$

where Q_{SWR} , Q_{LWR} , Q_{LAT} and Q_{SEN} represent shortwave radiative flux, longwave radiative flux, latent heat flux and sensible heat flux, respectively. The convention in this paper is that the positive heat flux means heat gain for the ocean and the negative for heat loss. The shortwave

radiative heat flux at the sea surface can be expressed further as the sum of the clear-sky radiative heat flux (Q_{CSR}) and cloud radiative forcing (Q_{CRF}) components:

$$Q_{SWR} = Q_{CSR} + Q_{CRF}. \quad (3)$$

Note that the radiative heat flux associated with cloud is difficult to measure. Therefore, we first obtain the clear sky radiative heat flux data from the NCEP/NCAR global reanalysis-1 (NCEP1, Kalnay et. al. 1996), then Q_{CRF} is computed by subtracting the NCEP1 clear sky radiative heat flux from the total shortwave heat flux of SHC data (Grist and Josey, 2003). The latent heat flux can be also divided into components:

$$Q_{LHF} = \overline{Q}_{LHF} + Q_{LAT(T)} + Q_{LAT(W)} + Q_{LAT(S)}, \quad (4)$$

where the first term in the RHS is the annual mean, and other three terms represent the SST-humidity-induced, wind speed-induced and the synoptic latent heat flux components, respectively. These could be written as

$$Q_{LAT(T)} = \rho L C_E |\overline{U}| q'_a - q'_s, \quad (5)$$

$$Q_{LAT(W)} = \rho L C_E |U'| (\overline{q}_a - \overline{q}_s), \quad (6)$$

$$Q_{LAT(S)} = \rho L C_E |U'| q'_a - q'_s, \quad (7)$$

where the variables with overbars indicate the annual mean and the variables with primes indicate the perturbation from the annual mean, L is the latent heat of evaporation (2.47×10^6 J/kg), C_E is the transfer coefficients for latent heat, U is the wind speed at $z=10$ m, q_a is specific humidity at $z=10$ m and q_s is the saturation specific humidity.

In the following section, the heat flux equations derived here are used to describe the annual heat budget cycle of the WHWP. The heat flux terms in (1) - (7) are obtained by first computing them at each time step during the model integration of the year 15, then taking the monthly

averages, thus the advective heat flux divergence term (Q_{ADV}) contains both mean and eddy contributions.

4. Annual heat budget cycle of the WHWP

a. Eastern North Pacific (ENP)

The first panel in Figure 2 shows the observed versus simulated seasonal cycle of the volume-averaged temperature for the ENP slab. The observed slab temperature is obtained from the World Ocean Atlas 2001 (WOA01) climatology (Conkright et al., 2002). The depth of the slab is taken as 20m, which is the approximate depth of 27.5°C for the ENP (EL05). The seasonal cycle of the temperature is quite regular, increasing from January to April, and decreasing in other months. The simulated slab temperature is positively biased, with the annual mean offset of $\sim 0.21^\circ\text{C}$. For future reference, the three months prior to the peak month is referred to as the onset phase (FMA), the three months centered at the peak month as the peak phase (AMJ) and the three months after the peak month as the decay phase (JJA), hereafter.

The slab heat budget cycle shown in the second panel indicates that, during the onset phase, the net surface heat flux ($Q_{NET}+Q_{SWP} = 50.4\text{W/m}^2$) forces the warming of the ENP slab while the diffusive heat flux (-14.2W/m^2) and advective flux divergence (-11.9W/m^2) damp out the heat. The decay phase starts after the peak in May and the rapid reduction of the surface net heat flux ($Q_{NET}+Q_{SWP}=5.3\text{W/m}^2$) helps the ENP to cool off. The diffusive (-6.5W/m^2) and advective cooling (-9.2W/m^2) is slightly less intense in the decay phase. The horizontal component of the advective heat flux divergence is a cooling term during the onset (-2.9W/m^2) and peak (-1.2W/m^2) phases, but much weaker than the vertical component.

The third panel shows the surface heat flux components, and the fourth the components for the shortwave radiative heat flux and the latent heat flux. For easier comparison among the terms, the annual mean components are removed and only the deviations from the annual mean are shown in the two panels. The monthly variations of the sensible heat and the longwave radiation are relatively small in comparison to the shortwave radiative heat flux and latent heat flux variations. Clearly, the rapid increase in net surface flux from December to March is due to the intensifying shortwave radiation. As noted in EL05, the cloud radiative forcing then increases very rapidly from the onset to the decay phase, standing out as the major factor in reducing the net surface flux and allowing the warm pool to cool off. Note that the clear-sky radiative heat flux remains strong till September. But, the increased cloudiness associated with the Pacific ITCZ approaching from the south and the onset of the monsoon from the southwest blocks much of the shortwave radiation during the decay phase, indicating that the shielding effect of deep convective clouds is a critical factor in cooling off the ENP as hypothesized by Ramanathan et al. (1995) for the Indo-Pacific warm pool.

The SST-humidity-induced latent heat flux largely follows the slab temperature cycle, thus being intensified during the peak months of the ENP slab. However, the wind forcing over ENP is weaker during the onset and peak phases but stronger during the decay phase. The total latent heat flux, therefore, increases in the peak and decay phases, providing the moisture seed to the atmosphere aloft needed for the tropical convection in boreal summer, at the same time as it helps to cool the ENP warm pool. An interesting point is that the reduction of wind speed during the peak phase fits the description of the convection-evaporation negative feedback (CE feedback hereafter) known to be important in the Indo-Pacific warm pool dynamics (Zhang et al., 1995). The CE feedback argues that, once the tropical Pacific water is sufficiently warmed,

surface wind is weakened due to large-scale low-level air mass convergence accompanied by deep tropical convection. The CE feedback is supported by statistical evidence that evaporation tends to decrease (or at least does not increase) after reaching peak SST of 28°C over the tropical Pacific (Zhang and McPhaden, 1995).

One of our main goals is to better understand the role of the ocean in the annual cycle of the WHWP. Figure 3 (top panels) clearly shows that the vertical advective heat flux divergence (colored), which is particularly intense during the onset phase, is forced by the positive wind stress curl (contoured lines) associated with the winter-time mountain-pass jets that appear in the Gulfs of Tehuantepec and Papagayo (McCreary et al., 1989; Chelton et al., 2000). The positive wind stress curl remains strong during the peak and decay phases due to the southwest monsoon onset. Eventually, the vertical advective cooling in the region is responsible for the spawning of the Costa Rica Dome in boreal summer (Hoffmann et al., 1981). Xie et al., (2004) reported that the reduced SST over the Costa Rica Dome creates a hole with about 500km in diameter in the convective cloud system, thus reducing the local precipitation by half of its surrounding region in boreal summer.

The middle panels of Figure 3 show the rate of horizontal advective heat flux divergence above the slab base at 20m (colored) and the velocity vector averaged vertically for the upper 20m. It clearly shows that the cold upwelled water is advected northwestward into the Gulfs of Tehuantepec and Papagayo, but due to the advection of warm water from the equatorial Pacific, the area-averaged rate of horizontal advective heat flux divergence is relatively small in the ENP slab. Shown in the bottom panels is the vertical turbulent heat flux (colored) and the velocity shear (contoured) both measured at the slab base (20m). The region of large turbulent heat flux corresponds to the region of increased shear, suggesting that the ENP may be prone to shear

instability. This result supports the microstructure observation of the upper ocean conducted near 10°N, 95°W during the EPIC2001 field program (Raymond et al., 2004).

In summary, the ENP warm pool develops in the spring primarily in response to increasing solar radiation, aided by reduced evaporation. As the warm pool size and intensity peak in March-April and the Central and North American land masses warm, the southwest monsoon over the Panama Bight and the Mexican Monsoon get their start and cloud cover increases greatly for the remainder of the solar forcing season, ending in October. The reduced shortwave radiation at the surface, aided by increased evaporation, cause the warm pool to decay until the early months of the following year. Thus, the ENP warm pool aids in its own demise. Advective and diffusive processes are important in shaping the distribution of warm pool depth and SST.

b. Gulf of Mexico (GoM)

Figure 4 is the same as Figure 2 except for the GoM slab. The depth of the GoM slab is chosen to be 20m following EL05. The GoM slab undergoes warming during March to July and cooling in other months. The simulated slab temperature is positively biased, with the annual mean bias of $\sim 0.46^{\circ}\text{C}$, and its annual cycle amplitude is slightly underestimated. During the winter months, the GoM experiences an intense cooling at the surface due to frequent mid-latitude frontal passages, resulting in a convective adjustment that overturns cooler mixed layer water with warmer water below. The convective warming of the cold surface water explains the positive diffusive heat flux during the winter months. As in the case of the ENP slab, the shortwave radiative heat flux and the latent heat flux are the major forcing terms in the GoM slab. But, the cloud radiative forcing is nearly constant throughout the year, leaving the clear-sky radiation as the largest forcing mechanism for the GoM slab, aided by the secondary forcing of

latent heat flux. The SST-humidity-induced latent heat flux largely follows the slab temperature cycle thus peaking around August. However, due to the reduction of the wind speed between June and September, the wind-induced latent flux is minimized in the warm pool's peak months (JAS), canceling off the large SST-humidity-induced latent heat flux there. The total latent heat flux, therefore, increases from the onset (MJJ) to the decay (SON) phase. The advective heat flux divergence seems to be insignificant over the year and cools the GoM slightly during the onset (-3.2W/m^2) and peak (-8.6W/m^2) months, in agreement with the slab-integrated residual calculated by EL05 from observations. However, it is important to note that the current model has a limited ability in resolving the Loop Current, which may have a significant impact on the heat budget cycle of the GoM slab. A high-resolution model simulation is needed to have a detailed and reliable assessment of the impact of ocean dynamics on the GoM warm pool.

c. Caribbean Sea (CBN)

In spite of shallow warm pool depths along the northern coast of South America, caused by coastal upwelling, a very deep region south of Cuba results in significantly greater 27.5°C isotherm depths, overall, than in the other regions (EL05). Here, the depth of the CBN slab is taken as 40m, which is the approximate regionally averaged depth of the 27.5°C isotherm during the peak phase of the CBN warm pool (EL05). As shown in Figure 5, the warming of the CBN slab starts in early March as in the GoM slab, but continues into mid-September. The heat storage rate is much larger in the earlier stage of the warming (April and May) and weaker afterward (JJAS). The advective heat flux divergence is insignificant between March and April, but it becomes the major cooling source between June and September (-20.0W/m^2), contributing to the significant reduction in the heat storage rate during the period of otherwise maximum

development. The net effect is the reduced rate of increase of the slab temperature between June and September as shown in the first panel. During the decay phase (OND), the advective heat flux divergence becomes less important (-6.9W/m^2). The diffusive cooling rate is much smaller and does not vary much throughout the warming months between March and September, ranging between -4.9 and -9.1W/m^2 . During the winter the decay of the CBN warm pool is primarily due to the sharp decrease in surface solar radiation. As in the ENP and GoM slabs, the monthly variations of the shortwave radiation and latent heat flux dominate the surface heat flux cycle. But, the shortwave radiation does not show much variation between April and August, while the latent heat flux is minimized between April and June, leading to slightly larger net surface heat flux in the earlier stage of the warming months (AMJ). The clear-sky radiation appears to be the major forcing mechanism for warming and cooling of the CBN slab. The cloud radiative forcing increases slightly between May and July, but it does not contribute much to the slab heat budget. The SST-humidity-induced latent heat flux roughly follows the slab temperature pattern, showing its peak in October. But, the wind-induced latent heat flux is minimized during the peak phase, thus the total latent heat flux remains quite constant till mid-October. During the decay phase (OND) the wind-induced latent heat flux increases rapidly, while the SST-humidity-induced latent heat flux still remains strong. The total latent heat flux, therefore, increases during the decay phase.

Figure 6 is the same as Figure 3 except for the CBN. As shown in the top panels, predominant easterlies and positive wind curl in the southern Caribbean are mainly responsible for the coastal upwelling off the South American continent. The cold upwelled water is then carried northwestward via the Caribbean Current, cooling the northwestern portion of the Caribbean Sea. This spreading of the cold upwelled water is the critical factor that inhibits the

development of the warm pool over the CBN region during the onset and peak phases. Further study using available observational data is required to confirm this finding.

Shown in the last panel is the vertical turbulent heat flux (colored) and the velocity shear (contoured) both measured at the slab base (40m). The increased shear along the path of the Caribbean Current seems to be closely tied with the large turbulent heat flux there. The positive diffusive heat flux in the northern part of the CBN during the decay phase is associated with wintertime convection, as in the Gulf of Mexico.

One thing that distinguishes the CBN from the other warm pool regions is its large depth, which is due to isotherm depths south of Cuba that approach 100m. A likely explanation for the deep mixed layer is the convective mixing caused by heating deeper water at a greater rate than the surface. Over the deep portion of the CBN south of Cuba, weak to negative net heat flux at the sea surface due to occasional penetration of cold spells from the North American Continent, combined with deep penetration of shortwave radiation, provides a favorable condition for a shallow convection to occur (McGregor and Nieuwolt, 1998). The positive diffusive heat flux over the same area during the decay phase as seen in Figure 6 seems to support this explanation. Schneider et al. (1996) used a similar argument to explain why the western Pacific and Indonesian portion of the Indo-Pacific warm pool is deeper than the warm pool portion in the Indian Ocean. Another important factor that may influence the large warm pool depth south of Cuba is the Ekman convergence due to the negative wind stress curl on the northern side of the mean Caribbean low-level jet, which is persistent in all three phases of the CBN warm pool development (see Figure 6). The core of the jet roughly coincides with the zero wind stress curl line shown in Figure 6. Additionally, the deep portion of the CBN is located at the core of the North Atlantic subtropical gyre, thus geostrophy favors a rapid eastward deepening of the

isotherms east of the intense northward-flow south of the Yucatan Channel. The relative importance of these factors in shaping the deep warm pool depth south of the Cuba is not clear. We feel that this subject merits a separate analysis, thus it is not pursued further in this study.

In summary, the CBN warm pool develops in the late summer and fall primarily due to increasing solar radiation, helped by reduced evaporation in the early warming stage. The coastal upwelling off the South American continent and horizontal advection of the cold water by the Caribbean Current significantly reduces the warming rate of the CBN during the summer. The reduced shortwave radiation at the surface, aided by intensifying trade wind in the winter thus increased evaporation, is mainly responsible for the decay of the CBN warm pool in OND.

d. Equatorial Atlantic (EQA)

The EQA slab, located near the Gulf of Guinea and the eastern equatorial Atlantic, is unique from other WHWP regions because its annual cycle is greatly influenced by the ocean dynamics (*i.e.*, advective heat flux divergence). As shown in Figure 7, the annual onset and decay of the EQA slab is largely controlled by the interchange between the advective heat flux divergence and the surface heating retained within the warm pool (second panel). The diffusive heat flux is also quite large throughout year reaching up to -29.4W/m^2 in June increasing from onset (-11.7W/m^2) to decay (-27.6W/m^2) phase. The clear-sky radiation has two peaks, one in May and the other in September, with minima in-between. However, the boreal winter minimum (fourth panel) is offset by reduced evaporative heat loss (third panel), resulting in an annual cycle of net surface heating with only a summer minimum (second panel).

As in other WHWP slabs, the wind-induced latent heat flux increases during the cooling months, while the SST-humidity-induced latent heat flux largely follows the slab temperature

pattern. As a result, the total latent heat loss increases during the peak and decay phases, but its overall impact on the total heat budget is much less than the advective heat flux divergence term.

In boreal fall, the EQA slab gains intense heat from the atmosphere due to the much reduced air-sea temperature gradient over the region of the cold water tongue (Lee and Csanady, 1999a). The intensification of the advective cooling during the decay phase is associated with equatorial upwelling, which results in the appearance of the cold-water tongue in boreal summer, thus the horizontal component of the advective heat flux divergence ranging between -15.0 (Jun) and 4.9W/m^2 (Feb) is less significant than the vertical component although the eddy mixing is an important warming mechanism locally over the cold-water tongue region (Foltz et al., 2003; Vialard et al., 2001; Weingartner and Weisberg, 1991). The strong shear between the South Equatorial Current and the Equatorial Undercurrent is mainly responsible for the large turbulent heat flux there, as shown in a simplified ocean model study by Lee and Csanady (1999b).

5. Comparison with EL05

Table 1 compares the model-generated values of diffusive and advective heat flux for the peak phases to those in EL05. Note that the EQA region is not included in the table because the geographical extent of the EQA slab used in this study is different from that in EL05. The model estimates agree generally with EL05 in that both the diffusive and the advective flux divergences cool all three regions at rates of up to -20 W/m^2 . The model-generated diffusive heat flux is lower (less negative) than those obtained from the bubble residual. The most plausible explanation for the disagreement is that the horizontal eddy heat flux divergence is included as a part of the diffusive heat flux in the bubble-residual estimate, but it is a part of the horizontal

advective heat flux in the model-generated estimates (see section 3). Guided by this argument, it is likely that the horizontal eddy flux in the ENP is greater (more negative) than -3.7 W/m^2 .

Consistent with the explanation offered above, the model-generated advective heat flux divergence is larger (more negative) for the ENP and CBN than that of the bubble-residual estimate. By summing the two heat flux terms, Q_{DIF} and Q_{ADV} , the two estimates (EL05 and HYCOM), are in much better agreement with each other, with the overall bias for the three regions being less than 2.6 W/m^2 .

6. Summary and Discussions

This study takes an alternate approach to that of EL05 for estimating the warm pool heat budget. EL05 dealt only with observations and the heat budget integrated over conterminous warm pool regions to estimate total diffusive heat flux across a bounding isotherm as a residual; they then used a slab approach in each subregion (Figure 1) to derive the total advective heat flux divergence as a residual by treating the diffusive flux as a known input. However, because the diffusive flux can only be estimated for the peak warm pool season when the warm pool can be defined by a reasonable isotherm, only peak season estimates of the heat budget could be made. By using a HYCOM-based model simulation of the warm pool optimized against observations (LEW05) we have been able to estimate all terms of the heat budget explicitly as functions of time and space, then integrating them over the subregional slabs. The analysis gives a complete annual cycle of the heat budgets by region and in most instances it confirms the EL05 estimates of diffusion and advective heat flux divergence for the peak seasons within acceptable limits.

One thing learned in this study is that the WHWP cannot be considered as a monolithic whole with a single set of dominating processes that explain its behavior. The four regions

considered are each unique in terms of the atmospheric and/or oceanic processes that dominate the corresponding heat budgets. In all cases some combination of surface fluxes is important, mainly clear sky radiation and evaporation. In the ENP region cloud cover plays a crucial role by modifying the clear sky radiation, and ocean upwelling in the Costa Rica Dome connected to surrounding areas by horizontal advection offers a persistent yearlong cooling mechanism. The GoM is marked by a process of winter overturning that warms the upper layer by convection, while advection is of little importance. The Caribbean is affected by vertical and horizontal advection within and away from the coastal upwelling zone off northern South America during the onset and peak phases slowing down the warming considerably. And advective processes associated with the equatorial cold tongue dominate the EQA region.

Common to all four WHWP regions is the reduction of wind speed in the peak phase, suggestive of a convection-evaporation feedback known to be important in the Indo-Pacific warm pool dynamics (Zhang et al., 1995). During the peak phase, the air-sea temperature (humidity) gradient is maximized, but the latent heat flux (moisture flux) is less effective due to the reduced wind speed. During the decay phase, the wind speed increases again and thus the latent heat flux increases, providing an important cooling mechanism for the WHWP.

This study demonstrates that an OGCM simulation is a useful tool for quantifying and understanding the thermodynamics of the warm pool more completely and effectively than is possible using only observational data. Although we found no evidence that the advective heat flux divergence is important in the GoM, a high-resolution model simulation is required to better assess the impact of the Loop Current there. Similarly, the high-resolution simulation will be also useful to explore the influence of the warm North Brazil Current Rings entering into the CBN basin. In future work, direct estimates of advective fluxes from available observational data

combined with the high-resolution model simulation will be used to validate the model results discussed here.

Acknowledgements. Our thanks to George Halliwell for his help on implementing the heat budget computation routine in HYCOM and to Rick Lumpkin, Alberto Mestas-Nuez and Libby Johns for the pre-submission reviews of the manuscript. This research was supported by the NOAA PACS/GAPP Program through awards under Cooperative Agreement NA67RJO149 to the Cooperative Institute for Marine and Atmospheric Studies.

References

- Bleck, R., 2002. An oceanic general circulation model framed in hybrid isopycnic-Cartesian coordinates. *Ocean Model.* 4, 55–88.
- Conkright, M. E., T. D. O'Brien, T. P. Boyer, C. Stephens, R. A. Locarnini, H. E. Garcia, P. P. Murphy, D. Johnson, O. Baranova, J. I. Antonov, R. Tatusko, R. Gelfeld, and I. Smolyar, 2002: World Ocean Database 2001, CD-ROM Data Set Documentation. Silver Spring, MD, National Oceanographic Data Center, 137 pp.
- Enfield, D. B. and S.-K. Lee, 2004: The heat balance of the Western Hemisphere Warm Pool. *J. Climate*, Submitted.
- Foltz G. R., S. T. Grodsky, and J. A. Carton, 2003: Seasonal mixed layer heat budget of the tropical Atlantic Ocean. *J. Geophys. Res.*, 108, 3146, doi:10.1029/2002JC001584.
- Grist, J. P. and S. A. Josey, 2003: Inverse Analysis Adjustment of the SOC Air-Sea Flux Climatology Using Ocean Heat Transport Constraints. *J. Climate*, 16, 3274-3295.

- Halliwel, G. R., 2004: Evaluation of vertical coordinate and vertical mixing algorithms in the HYbrid-Coordinate Ocean Model (HYCOM). *Ocean. Model.*, 7, 285-322.
- Hofmann, E. E., A. J. Busalacchi and J. J. O'Brien, 1981: Wind generation of the Costa Rica Dome. *Science*, 214, 552-554.
- Kalnay, E., M. Kanamitsu, R. Kistler, W. Collins, D. Deaven, L. Gandin, M. Iredell, S. Saha, G. White, J. Woollen, Y. Zhu, M. Chelliah, W. Ebisuzaki, W. Higgins, J. Janowiak, K. C. Mo, C. Ropelewski, J. Wang, Leetmaa, R. Reynolds, R. Jenne, and D. Joseph, 1996: The NCEP/NCAR 40-year Reanalysis Project. *Bull. American Meteorol. Soc.*, 77, 437-471.
- Large, W.G., McWilliams, J.C., Doney, S.C., 1994: Oceanic vertical mixing: a review and a model with a non-local boundary layer parameterization. *Rev. Geophys.* 32, 363–403.
- Lee, S.-K. and G.T. Csanady, 1999a: Warm water formation and escape in the upper tropical Atlantic Ocean: 1. A literature review. *J. Geophys. Res.*, 104, C12, 29,561-29,571.
- and G.T. Csanady, 1999b: Warm water formation and escape in the upper tropical Atlantic Ocean: 2. A numerical model study. *J. Geophys. Res.*, 104, C12, 29,573-29,590.
- , D. B. Enfield, C. Wang, 2005: OGCM sensitivity experiments on the annual cycle of Western Hemisphere Warm Pool. *J. Geophys. Res.*, Submitted.
- McCreary, J. P., H. S. Lee, and D. B. Enfield, 1989: The response of the coastal ocean to strong offshore winds: With application to circulations in the Gulfs of Tehuantepec and Papagayo. *J. Mar. Res.*, 47, 81-109.
- McGregor, G. R. and S. Nieuwolt, 1998: *Tropical climatology: An introduction to the climates of the low latitudes*, second edition, John Willey & Sons, Chichester, 339p.
- Niiler, P. P. and J. Stevenson, 1982: On the heat budget of tropical warm water pools. *J. Mar. Res.*, 40 (Suppl), 465-480.

- Ramanathan, V., B. Subasilar, G. J. Zhang, W. Conant, R. D. Cess, J. T. Kiehl, H. Grassl, and L. Shi, 1995: Warm pool heat budget and shortwave cloud forcing: A missing physics? *Science*, **267**, 499-503.
- Raymond, D. J., S. K. Esbensen, C. Paulson, M. Gregg, C. S. Bretherton, W. A. Peterson, R. Cifelli, L. K. Shay, C. Ohlmann, and P. Zuidema, 2004: EPIC2001 and the coupled ocean-atmosphere system of the tropical east Pacific. *Bull. American Meteorol. Soc.*, **85**, 1341-1354.
- Vialard, J., C. Menkes, J.-P. Boulanger, P. Delecluse, E. Guilyardi, M. J. McPhaden and G. Madec, 2001: A model study of oceanic mechanisms affecting equatorial Pacific sea surface temperature during the 1997-98 El Nino. *J. Phys. Oceanogr.*, **31**, 1649-1675.
- Wang, C. and D. B. Enfield, 2001: The Tropical Western Hemisphere warm pool. *Geophys. Res. Lett.*, **28**, 1635-1638.
- , 2003: A further study of the tropical Western Hemisphere warm pool. *J. Climate*, **16**, 1476-1493.
- Weingartner, T. J., and R. H. Weisberg, 1991: A description of the annual cycle in seas surface temperature and upper ocean heat in the equatorial Atlantic. *J. Phys. Oceanogr.*, **21**, 83-96.
- Xie, S.-P., H. Xu, W. S. Kessler and M. Nonaka, 2004: Air-sea interaction over the eastern Pacific warm pool: Gap winds, thermocline dome, and atmospheric convection. *J. Climate*, In press.
- Zhang, G. J. and M. J. McPhaden, 1995: The relationship between sea surface temperature and latent heat flux in the equatorial Pacific. *J. Climate*, **8**, 589-605.
- , V. Ramanathan, and M. J. McPhaden, 1995: Convection-Evaporation Feedback in the equatorial Pacific. *J. Climate*, **8**, 3040-3051.

Table 1. The model-generated values of diffusive and advective heat flux for the peak phases of the ENP, GoM and CBN regions are compared with those obtained in EL04. Note that the EQA region is not included in the table because the geographical extent of the EQA slab used in this study is different from that in EL05. The unit is W/m^2 .

Region	Q_{DIF}		Q_{ADV}		$Q_{DIF} + Q_{ADV}$	
	EL04	HYCOM	EL04	HYCOM	EL04	HYCOM
ENP	-23.6 ~ -13.6	-9.9	-3.3 ~ -1.3	-10.2	-26.6 ~ -14.9	-20.1
GoM	-14.7 ~ -7.9	-4.9	-15.1 ~ -5.4	-8.6	-29.8 ~ -13.3	-13.5
CBN	-9.3 ~ -4.3	-5.2	-8.5 ~ 0.7	-15.2	-17.8 ~ -3.6	-20.4

Figure captions

Figure 1. The model grid structure in the eastern tropical Pacific and the tropical Atlantic analysis domain (uniform 1° in zonal and variable in meridional direction; 0.5° at the equator increasing linearly to 1° at 40° latitude and 1° pole ward of 40°). The locations of the four subregions of the WHWP are also shown. Note that the entire model domain contains both Pacific and Atlantic Oceans between 100°E and 20°E , bounded north and south by 35°S and 65°N , respectively.

Figure 2. The seasonal cycle of the volume-averaged thermal flux properties in the ENP slab. The first panel shows the temperature, the second and third the heat budget and surface heat flux, respectively. The last panel shows the shortwave radiative heat flux and latent heat flux components. In the last two panels, the annual mean components are removed for easier comparison.

Figure 3. The top panels show the vertical advective heat flux divergence rate (colored) and wind stress curl (contoured) for the ENP slab. The middle panels show the rate of horizontal advective heat flux divergence above the slab base (colored) and the velocity vector averaged vertically for the upper 20m. Shown in the bottom panels is the vertical turbulent heat flux (colored) and the velocity shear (contoured) both measured at the ENP slab base (20m). The left column is for the onset phase (FMA), the center and the right for the peak (AMJ) and decay (JJA) phase, respectively. The units are W/m^2 for the heat flux terms, 10^7Nm^{-3} for the wind stress curl and 10^2s^{-1} for the shear.

Figure 4. Same as Figure 2 but for the GoM slab.

Figure 5. Same as Figure 2 but for the CBN slab.

Figure 6. The top panels show the vertical advective heat flux divergence rate (colored) and wind stress curl (contoured) for the CBN slab. The middle panels show the rate of horizontal advective heat flux divergence above the slab base at 40m (colored) and the velocity vector averaged vertically for the upper 40m. Shown in the bottom panels is the vertical turbulent heat flux (colored) and the velocity shear (contoured) both measured at the CBN slab base (40m). The left column is for the onset phase (JJA), the center and the right for the peak (ASO) and decay (OND) phase, respectively. The units are W/m^2 for the heat flux terms, 10^7Nm^{-3} for the wind stress curl and 10^2s^{-1} for the shear.

Figure 7. Same as Figure 2 but for the EQA slab.

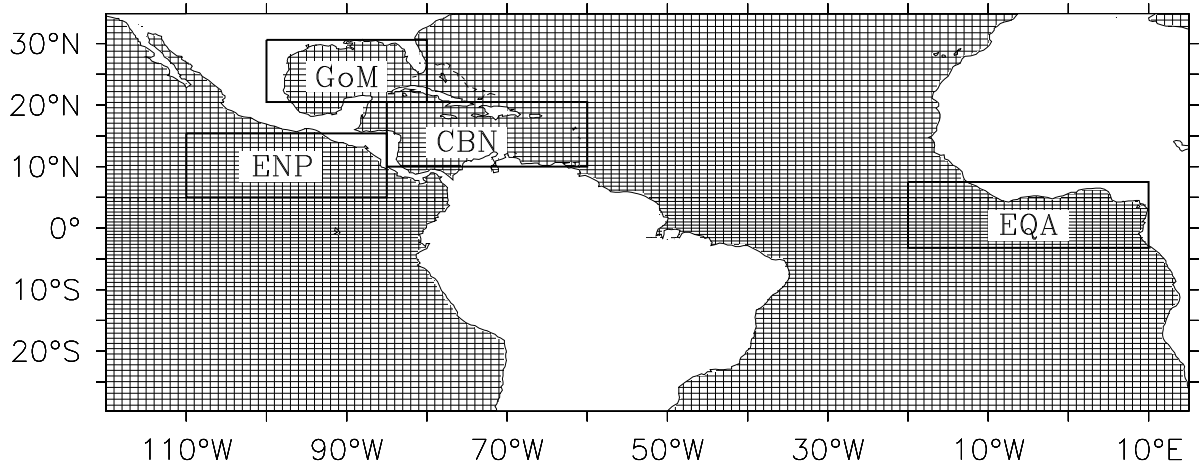


Figure 1

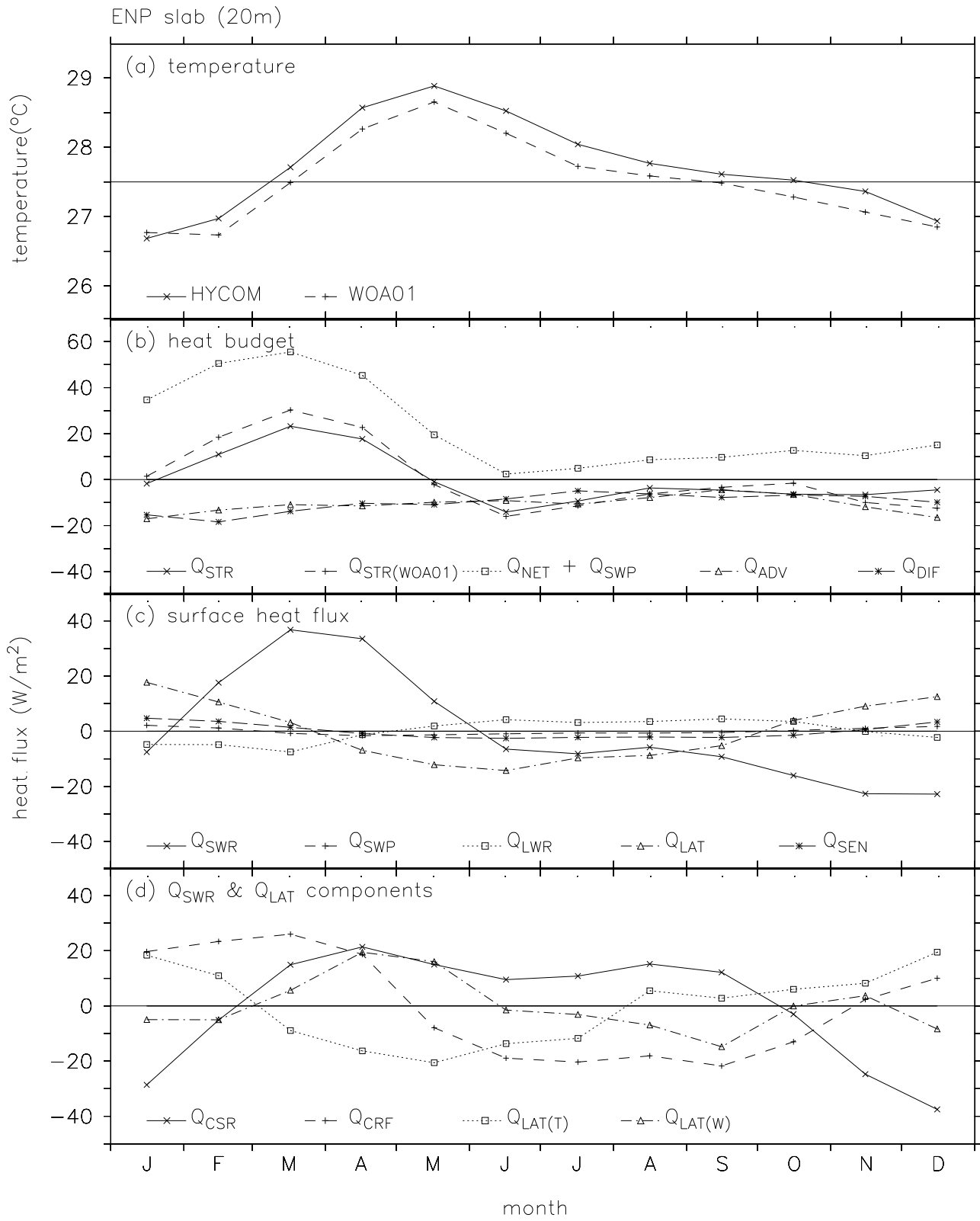


Figure 2

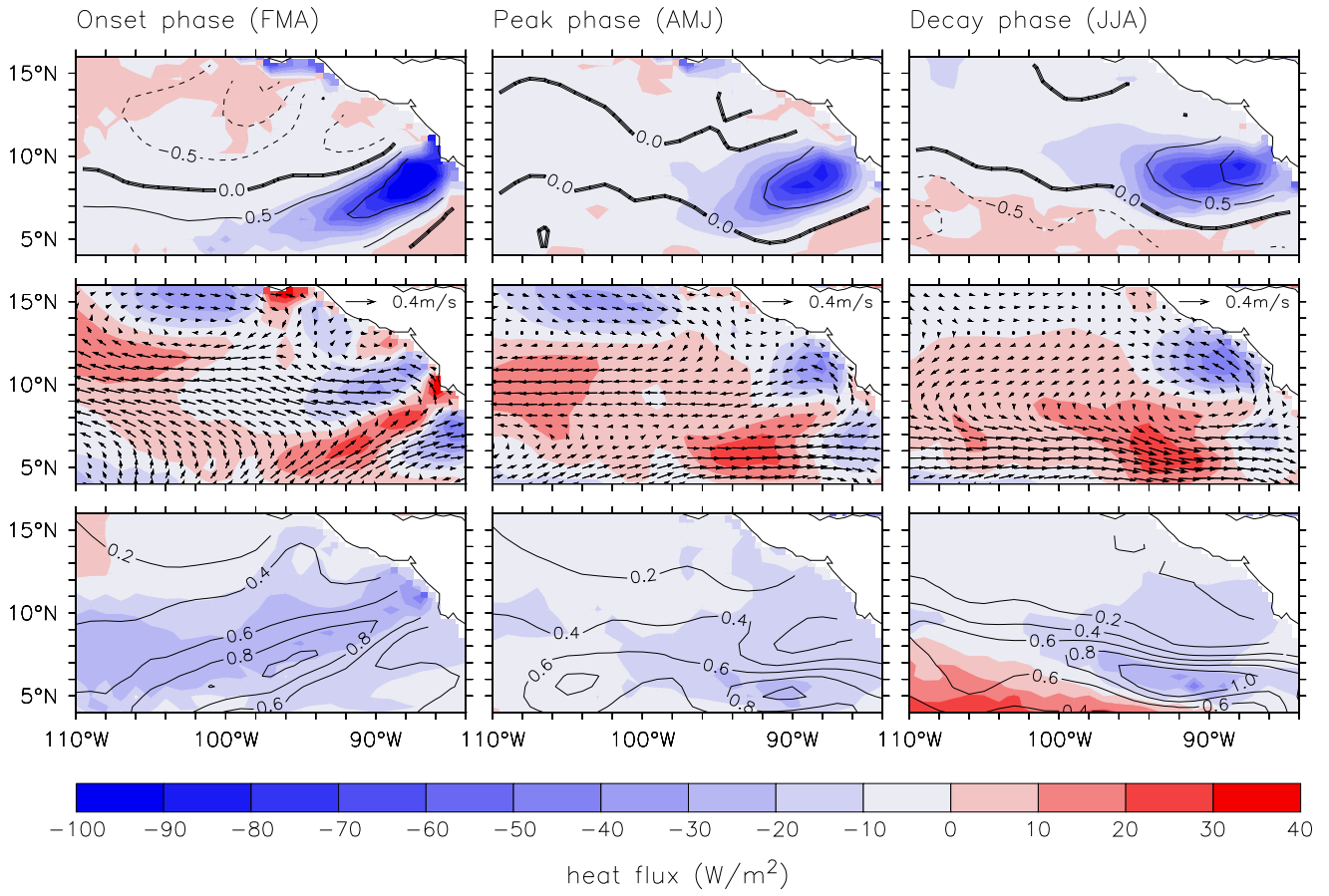


Figure 3

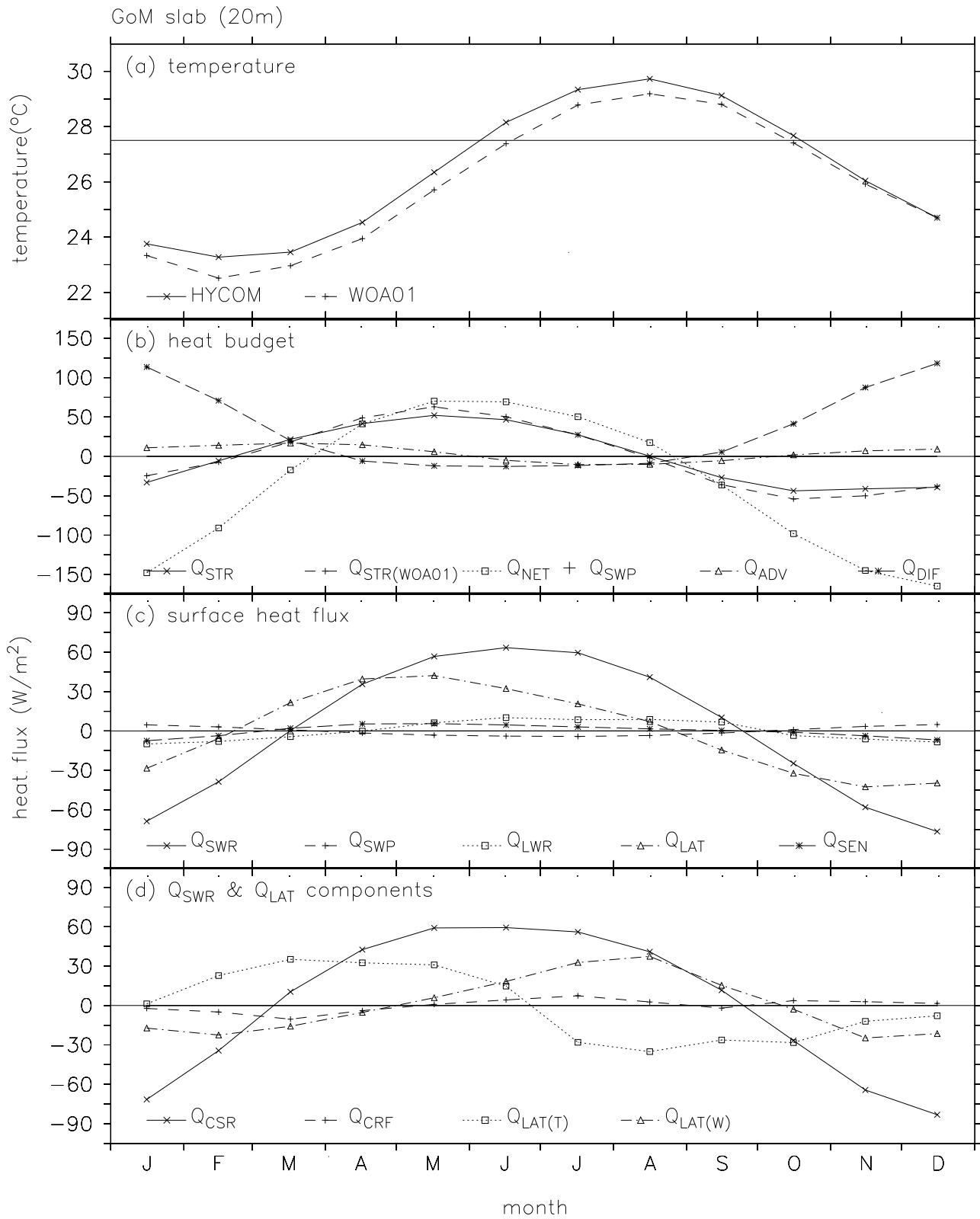


Figure 4

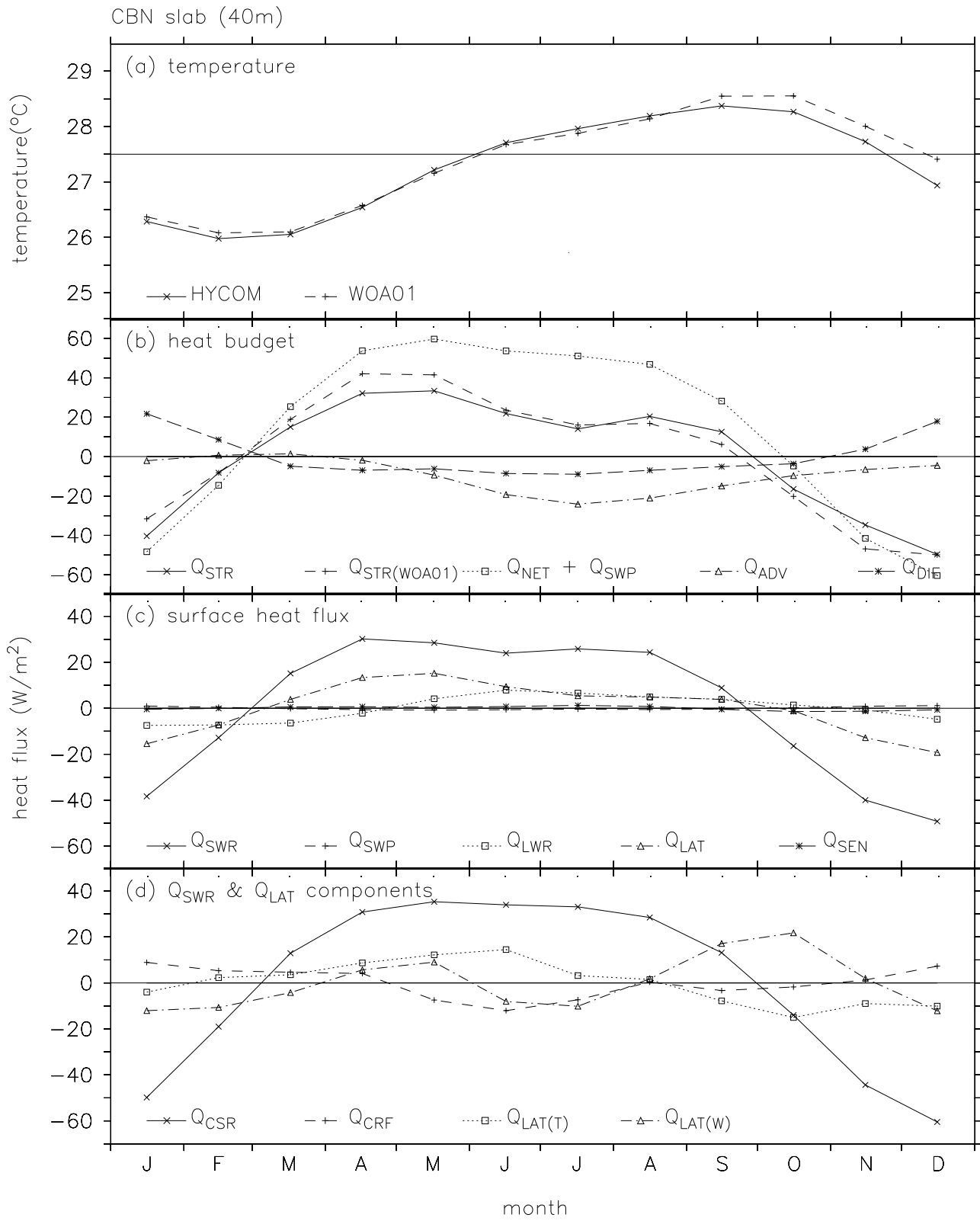


Figure 5

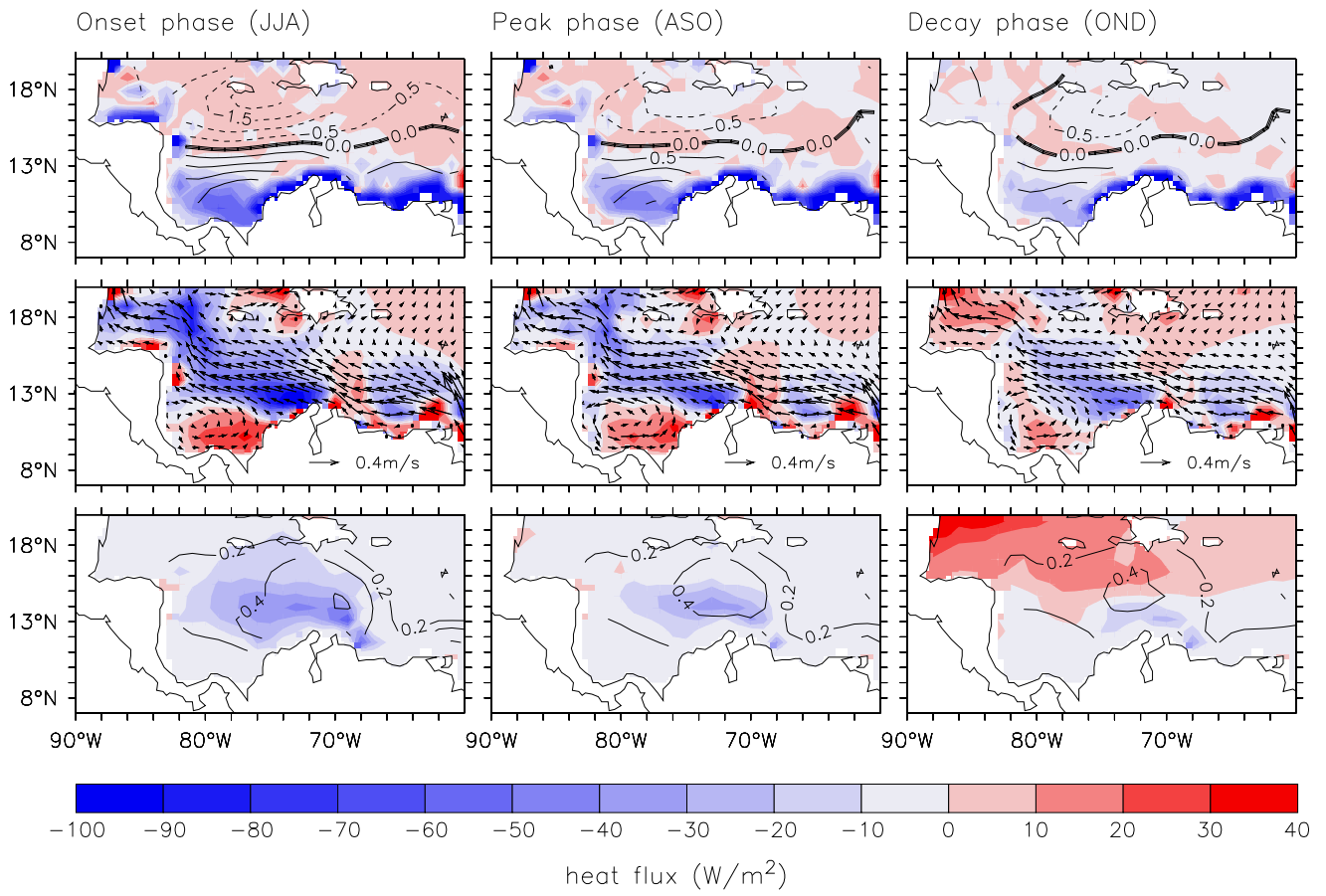


Figure 6

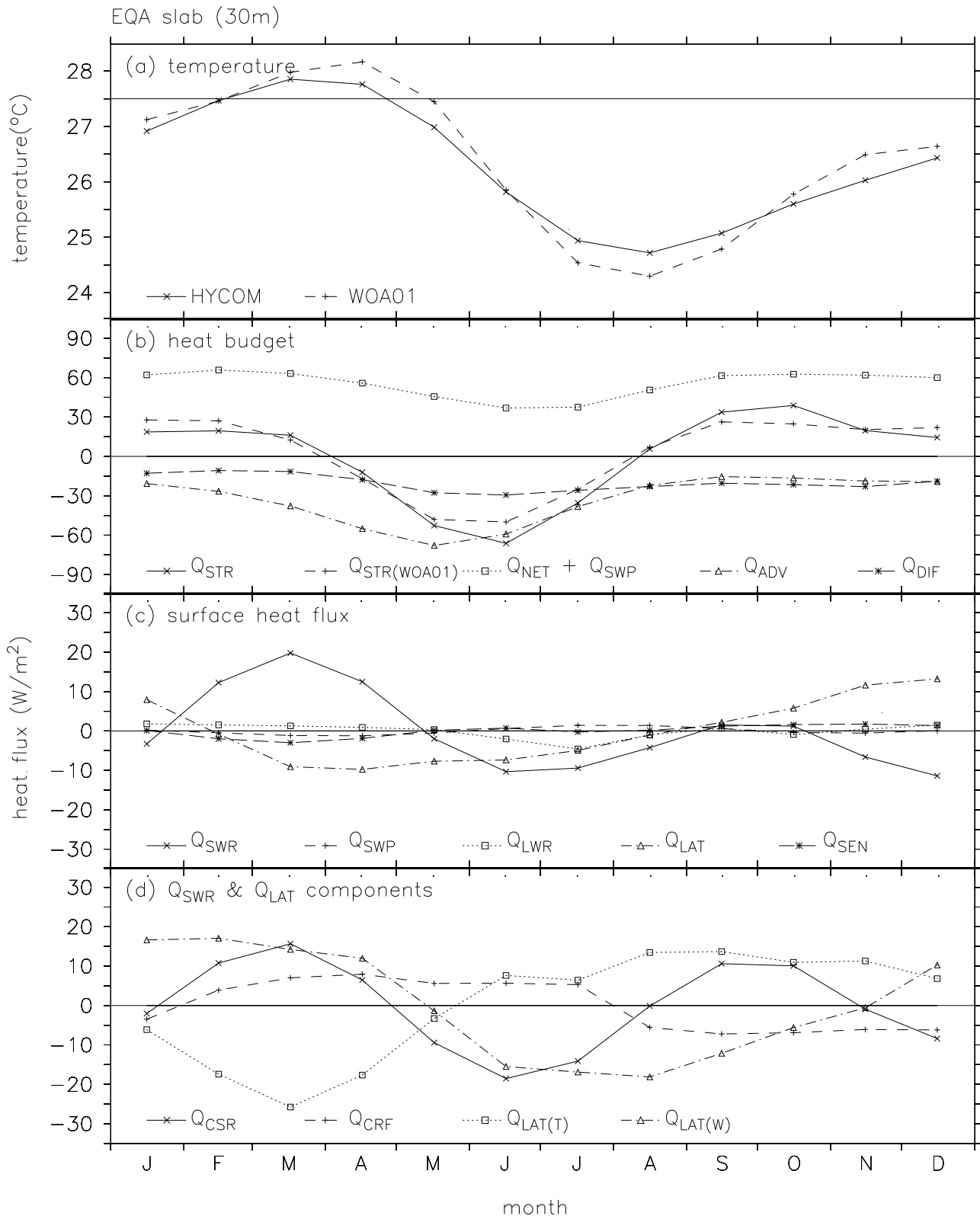


Figure 7